Nano Energy 68 (2020) 104347

Contents lists available at ScienceDirect

Nano Energy

journal homepage: http://www.elsevier.com/locate/nanoen

Communication

Stacking faults modulation for scattering optimization in GeTe-based thermoelectric materials

Li Xie [a,b,1], Yongjin Chen [c,1], Ruiheng Liu [a,b,*], Erhong Song [a], Tong Xing [a,b], Tingting Deng [a], Qingfeng Song [a], Jianjun Liu [a], Renkui Zheng [a], Xiang Gao [c,**], Shengqiang Bai [a,b,***], Lidong Chen [a,b]

[a] State Key Laboratory of High Performance Ceramics and Superfine Microstructure, Shanghai Institute of Ceramics, Chinese Academy of Sciences, Shanghai, 200050, China
[b] Center of Materials Science and Optoelectronics Engineering, University of Chinese Academy of Sciences, Beijing, 100049, China
[c] Center for High Pressure Science &Technology Advanced Research, Beijing, 100094, China

ARTICLE INFO

Keywords:
GeTe
Stacking faults
Scattering optimization
Thermoelectric materials

ABSTRACT

The enhancement of thermoelectric (TE) performance is essentially associated with optimizing the scattering effect of electron and phonon. Here, we demonstrate a stacking faults modulation strategy in GeTe materials to simultaneously realize high carrier mobility and low lattice thermal conductivity. Excess Cu doping in GeTe can significantly decrease the concentration of Ge vacancy layer and form a "vacancy/Cu–Cu/vacancy" sandwich-like stacking faults structure. As a result, the hole mobility is remarkably improved to nearly ~100 $cm^2 V^{-1} s^{-1}$ at room temperature due to the weakened carrier scattering from vacancy layer, which ensures superior electrical transport properties. Meanwhile, the sandwich-like stacking faults brings much stronger scattering effect on phonons, thus leading to extremely low lattice thermal conductivity of 0.38 $W m^{-1} K^{-1}$. With synergistically optimized scattering effect on carriers and phonons, a peak thermoelectric figure of merit over 2.0 is achieved in $Ge_{0.89}Cu_{0.06}Sb_{0.08}Te$ at 750 K. This work provides an effective strategy to realize selective scattering of phonons and carriers through 2D defect modulation, and makes up the important piece of multi-scale microstructure tailoring for TE materials.

1. Introduction

Nowadays, the problems of energy consumption and environmental pollution have aroused people's great concern. Thermoelectric technology is able to convert thermal energy into electricity by Seebeck effect, which can be used in waste heat recovery, offering an alternative method to overcome the challenges of energy sustainability [1–4]. The conversion efficiency of thermoelectric device is evaluated by material's dimensionless figure of merit zT, defined as $zT = S^2\sigma T/(\kappa_e + \kappa_L)$, where S, σ, κ_e, κ_L, and T are Seebeck coefficient, electrical conductivity, electronic thermal conductivity, lattice thermal conductivity, and absolute temperature, respectively [5]. A high performance thermoelectric material requires synergistically enhanced electrical transport properties (power factor) and reduced thermal conductivity.

The TE performance is essentially associated with the transportation of electrons and phonons for semiconducting thermoelectric materials [6–9]. Because the above-mentioned thermoelectric parameters are interdependent, a high electrical performance, namely the maximal power factor, can only be achieved within a narrow range of carrier concentration [10,11], or further enhanced by band structure manipulation [12,13], which are realized by chemical doping or alloying. However, doping or alloying introduces different kinds of defects, which will inevitably scatter the conductive carriers and thus suppress the mobility of carriers, though it also can scatter phonons to some extent [14–16]. Therefore, how to modulate and optimize the effect of introduced defects on electron and phonon scattering is the key to improve

* Corresponding author. State Key Laboratory of High Performance Ceramics and Superfine Microstructure, Shanghai Institute of Ceramics, Chinese Academy of Sciences, Shanghai, 200050, China.
** Corresponding author.
*** Corresponding author. Center of Materials Science and Optoelectronics Engineering, University of Chinese Academy of Sciences, Beijing, 100049, China.
E-mail addresses: liurh@mail.sic.ac.cn (R. Liu), xiang.gao@hpstar.ac.cn (X. Gao), bsq@mail.sic.ac.cn (S. Bai).
[1] These authors contributed equally to this work.

https://doi.org/10.1016/j.nanoen.2019.104347
Received 30 September 2019; Received in revised form 24 November 2019; Accepted 29 November 2019
Available online 3 December 2019

thermoelectric properties. Up to now, to achieve selective scattering of electrons and phonons, i.e. noticeably scattering phonons and scarcely affecting electrons, multiscale scattering sources, such as 0D point defects [17–19], 1D dislocations [20,21], 2D superlattice [22] and twin boundary [23,24], as well as 3D nanoinclusions and nanopores [25–27], are intentionally constructed and widely investigated.

Stacking faults are induced by the abnormal periodic stacking sequence of 2D layers in crystal lattice, which potentially provide supplementary scattering effect among multiscale scattering sources. Stacking faults are typical 2D lattice defects in lots of crystalline TE materials, such as GeTe, which has attracted researcher's attention due to its high band degeneracy in both rhombohedral and cubic phase [28]. Because of large mismatch between Ge and Te atoms, high concentration of Ge vacancy layers exists in pristine GeTe compound, leading to an extremely higher carrier concentration ($\sim 10^{21}$ cm^{-3}) than the optimal value [29]. Therefore, most reported optimization strategies to improve thermoelectric properties of GeTe are mainly through reducing high hole concentration [10,30], combined with a convergence of multiple sub-bands [16,31]. It has been demonstrated that aliovalent element Bi and Sb are the most effective dopants to reduce carrier concentration to the optimal range $\sim$ 1–3 $\times$ 10^{20} cm^{-3} [32–34]. Together with Sb or Bi doping, co-doping of Mn/Mg, In or Cd, can effectively optimize carrier concentration and band structure [16,35–37]. However, doping or alloying inevitably increases the concentration of point defects or stacking faults [16,35,37], thus the carrier mobility in GeTe is severely reduced due to the increased scattering of defects, which offsets the benefits from band convergence and phonon scattering. Recently, Dong and Bu reported that excess Ge doping and Cu_2Te alloying could successfully reduce the carrier concentration through depressing the formation of Ge vacancy [19,38]. Therefore, simultaneously suppressing the formation of intrinsic Ge vacancy layers to obtain high carrier mobility and effectively scattering phonons to achieve low lattice thermal conductivity in GeTe are the most favorable route for further promotion of thermoelectric performance.

In the present work, we proposed a stacking faults modulation strategy to optimize the scattering effect both for carriers and phonons. Firstly, we found that, the excess Cu doping can change the morphology of Ge vacancy layer by forming a "vacancy/Cu–Cu/vacancy" sandwich-like stacking faults structure, and the concentration of simple one-fold Ge vacancy layers is significantly reduced (Fig. 1a). As a result, the hole mobility is remarkably improved to nearly $\sim$100 cm^2 V^{-1} s^{-1} at room temperature, which ensures superior electrical transport properties. Meanwhile, the replacement of the simple one-fold Ge vacancy layer by sandwich-like stacking faults brings much stronger scattering effect on phonons, thus leading to a depression of lattice thermal conductivity. Together with Sb doping, the lattice thermal conductivity is greatly decreased to 0.38 W m^{-1} K^{-1}, approaching the amorphous limit of GeTe. Therefore, the peak zT value exceeding 2.0 at 750 K and zT_{ave} value of 1.35 over 400–800 K are predictably achieved in $Ge_{0.89}Cu_{0.06}Sb_{0.08}Te$ (Fig. 1b–c), indicating that the stacking faults modulation can be an effective strategy to realize selective scattering of phonon and carriers.

2. Experimental section

2.1. Sample preparation

Polycrystalline samples with nominal compositions of $Ge_{1-x-y}Cu_{2x}Sb_yTe$ ($x = 0$, 0.01, 0.015, 0.02, 0.03, $y = 0$; $x = 0.03$, $y = 0.04$, 0.06, 0.08, 0.10) were synthesized by traditional melting-annealing-spark plasma sintering (SPS) method. High purity raw materials, including Ge (pieces, 99.999%, Alfa Aesar), Cu (shots, 99.999%, Alfa Aesar), Sb (shots, 99.9999%, Alfa Aesar), Te (pieces, 99.999+%, Alfa Aesar) were weighed in stoichiometric ratios and sealed in evacuated quartz tubes (diameter of 10 mm). The mixtures were heated to 1373 K in 11 h and maintained at this temperature for 12 h to ensure complete melting of all elements. The tubes were quenched in cold water, and then annealed at 873 K for 5 days. The obtained ingots were grinded into fine powders, then loaded into a graphite die with the diameter of 10 mm, and consolidated by SPS (Sumitomo SPS-2040) in vacuum at 813 K for 10

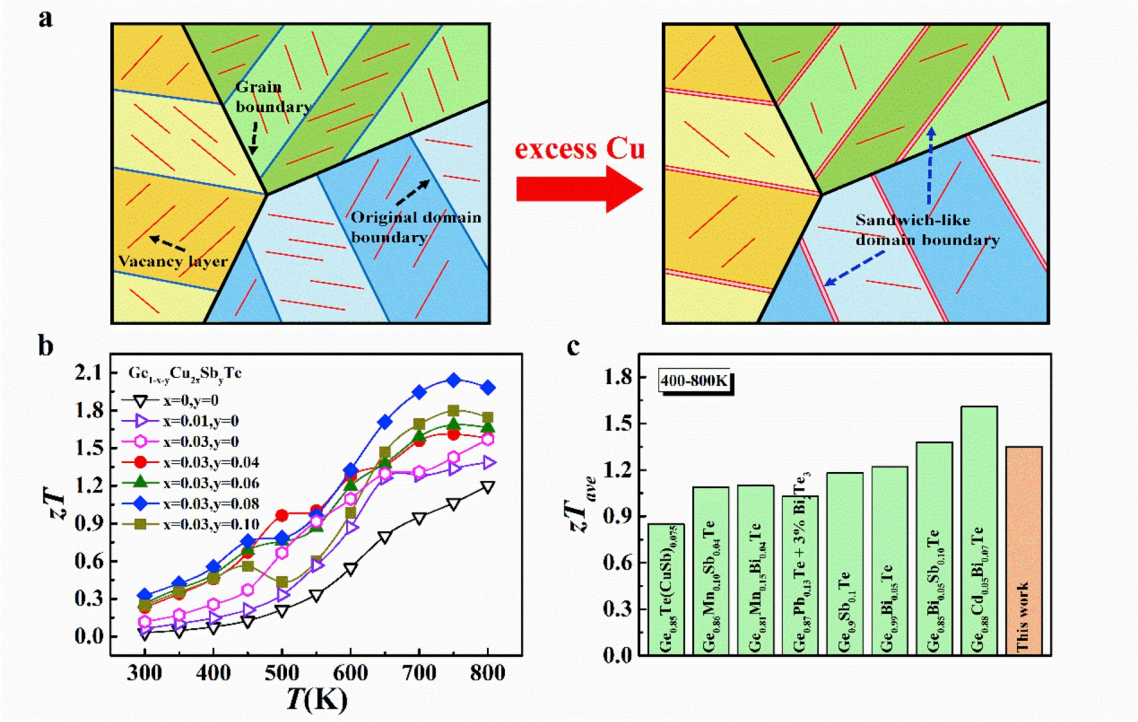

Fig. 1. (a) Schematic diagram showing the morphology and concentration of stacking faults within grains influenced by excess Cu doping. (b) Temperature dependence of the figure of merit zT for $Ge_{1-x-y}Cu_{2x}Sb_yTe$. (c) Comparison of the average figure of merit zT_{ave} at 400–800 K for $Ge_{0.89}Cu_{0.06}Sb_{0.08}Te$ and several literatures [11,16,32–34,37,39,40].

min under a pressure of 50 MPa to obtain fully dense bulk samples.

2.2. Materials characterizations and measurements

Powder X-ray diffraction analysis (D8 Advance, Bruker; Cu Kα: λ = 1.5406 Å) was performed to identify the phase composition of samples. The Rietveld refinements of the XRD patterns were performed using Fullprof software. The morphology and microstructure were investigated with scanning electron microscopy (SEM, ZEISS Supra 55) and aberration-corrected transmission electron microscopy (Cs-corrected TEM, FEI G2 Themis, 300 KeV). High-density samples obtained after SPS were cut into bars with dimensions of ~2 mm × 2 mm × 8 mm, and pellets with diameter of 10 mm and thickness of ~1.5 mm for thermoelectric performance characterization. High temperature electrical conductivity (σ) and Seebeck coefficient (S) were measured simultaneously on the bars using commercial instrument system (ZEM-3, ULVAC-RIKO) under a helium atmosphere from 300 K to 800 K. The thermal conductivity (κ) was calculated using the formula $\kappa = \rho\ C_p\ D$, where the density (ρ) of pellets was determined by Archimedes method and the relative density of all samples were above 98% at room temperature, the specific heat capacity (C_p) was estimated by Dulong-Petit law, the thermal diffusivity (D) was measured on the pellets in an argon atmosphere by laser flash system (LFA 457, Netzsch), and the Cape-Lehman method with pulse correction was used to analyze the thermal diffusivity data. The Hall coefficient (R_H) was measured with a five-probe configuration under a magnetic field of −3 T–3 T using a Physical Property Measurement System (PPMS-Quantum Design). And high temperature Hall coefficient (R_H) was measured with a four-probe van der Pauw technique under AC field using a Hall Effect Measurement System (Lake Shore 8400 Series). The carrier concentration (n) and carrier mobility (μ) were calculated from $n = 1/eR_H$ and $\mu = \sigma/ne$, where e is the elementary charge and σ is the electrical conductivity.

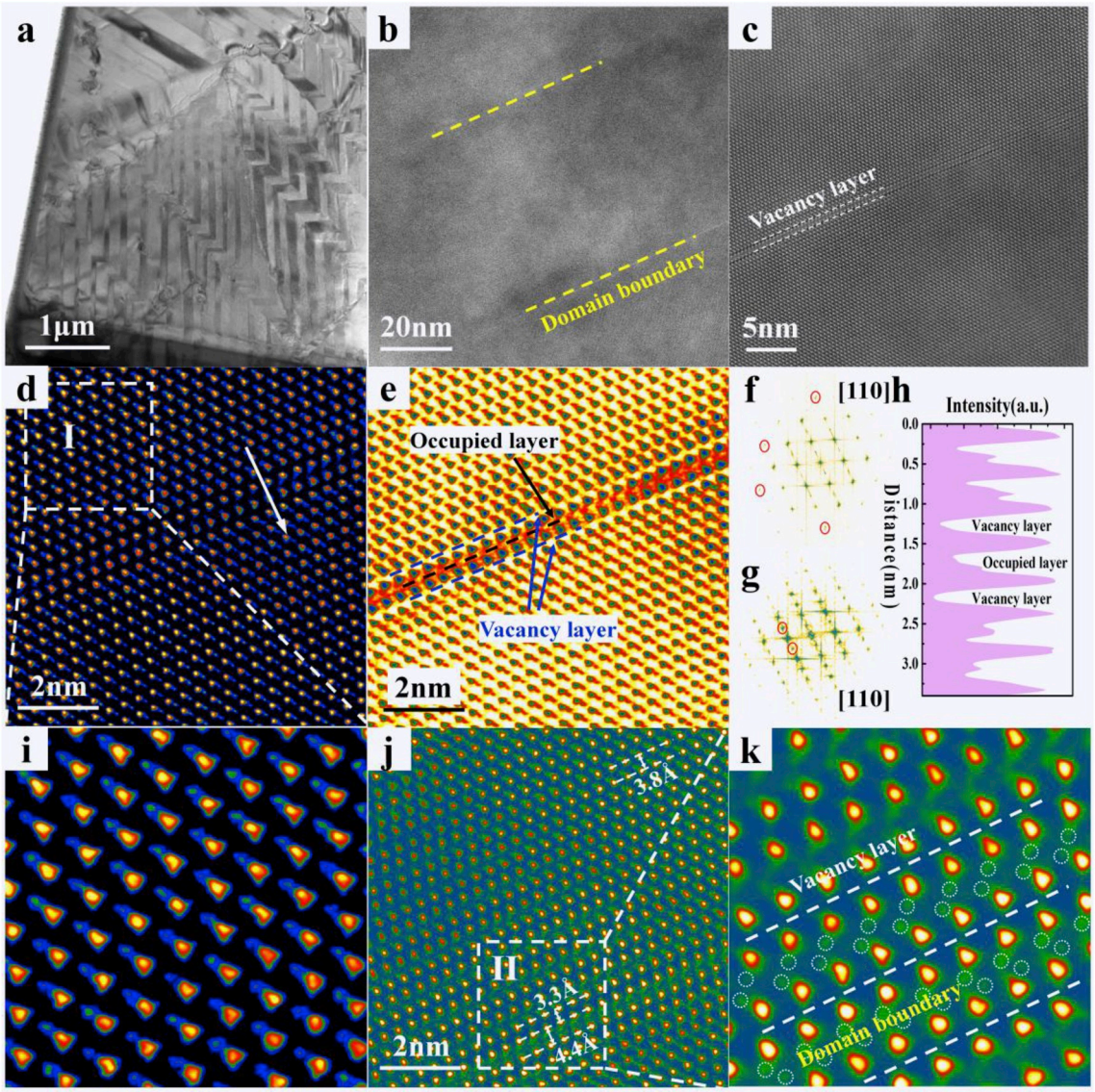

Fig. 2. Microstructure of $Ge_{0.91}Cu_{0.06}Sb_{0.06}Te$ sample. (a) Bright-field TEM image showing domain variants, called herringbone structure. (b)Medium-sized HAADF-STEM image of partial region of a single domain, and (c) HAADF-STEM image of a domain boundary. (d) HAADF and (e) corresponding ABF-STEM images showing the atom configuration of another typical domain boundary. (f) and (g) showing the corresponding FFT-transformed electron diffraction pattern of the area in (c) and (j), respectively. (h) Line profile showing the image intensity along the arrow in (d). (i) Enlarged view of the framed area I in (d) to show the atom arrangement of the matrix. (j) HAADF-STEM image showing atom structure with the formation of vacancy layers nearby a domain boundary, and (k) magnified region II in (j) showing the occupation of Cu atoms in vacancy layer. Colors are only used to improve the visual effect of images, unless specified, and original images are shown in Fig. S4.

3. Result and discussion

Polycrystalline samples with nominal compositions of $Ge_{1-x-y}Cu_{2x}Sb_yTe$ were synthesized by traditional melting-annealing-spark plasma sintering (SPS) method. Fig. S1a is the room temperature powder X-ray diffraction (PXRD) patterns of $Ge_{1-x-y}Cu_{2x}Sb_yTe$ samples. The main diffraction peaks of all samples can be indexed to low temperature rhombohedral phase of GeTe, with trace amount of Ge precipitates as a secondary phase, which is a common phenomenon in the GeTe synthesis process [35,41]. In samples with $x \geq 0.04$, $y = 0$, a little amounts of impurity phase Cu_2Te is detected in the PXRD pattern, proving that the solubility limit is x~3%. Increasing doping content of Sb with fixed $x = 0.03$, the double peaks in 2θ range around 23–27° and 41–45°gradually merge, indicating the crystal structure of GeTe transforms from rhombohedral structure (*R-3m*) to cubic rocksalt structure (*Fm-3m*). In order to further characterize the influence of (Cu,Sb) co-doping on crystal structure, lattice parameter (a) and interaxial angle (α) are estimated by Rietveld refinements based on PXRD data of $Ge_{1-x-y}Cu_{2x}Sb_yTe$ samples. Both lattice parameter and interaxial angle increase slightly as x rises, shown in Fig. S1b. When varying Sb-doping concentration, lattice parameter stays almost unchanged and interaxial angle is pushed to approach 90°, proving that the lattice approaches cubic structure [28]. The energy dispersive spectroscopy (EDS) elemental mapping for $Ge_{1-x-y}Cu_{2x}Sb_yTe$ samples shows that all constituent elements are uniformly distributed at the microscale, with the existence of Ge precipitates (Fig. S3), further confirming the formation of solid solutions of the matrix.

The microstructure characterized by TEM investigation was carried out on the sample $Ge_{0.91}Cu_{0.06}Sb_{0.06}Te$. Fig. 2a displays a regular arrangement of domain variants with bright and dark contrasts, referred as herringbone structures, which is a typical feature in the GeTe-based materials [42]. Aberration-corrected high angle imaging-mode annular dark field (HAADF) are employed to examine the detailed atomic configuration of the domain. As exampled in the magnified HAADF image (Fig. 2b), the domain is about 60 nm in width and the domain interior is free from dislocations or vacancy layers, showing rather a different microstructure with the literatures [31,32,37,43,44], in which the domain is usually accompanied by high density of Ge-vacancy or vacancy layers. Obviously, compared to previous reports, fewer defect layers are observed in the same size region in this work, which means that the formation of vacancy layers is suppressed.

The domain boundary has also been studied in detail. Fig. 2c is a zoomed version of a domain boundary, implied by the that orientations of the neighboring domains are different. And this is confirmed by a slight beam splitting of high-index diffraction spots along the [110] directions in the corresponding fast Fourier transform (FFT) electron diffraction pattern (Fig. 2f). Besides, the domain boundary seems to be composed of several layers of stacking faults. Fig. 2d and e are HAADF and annular bright field (ABF) images showing the atom configuration of another domain boundary, respectively. In the Z-contrast HAADF image, the intensity of atomic columns is roughly proportional to Z^2, the heavier Te ($Z = 52$) atoms show a much brighter contrast than that of Ge ($Z = 32$). Fig. 2d depicts a locally amplified domain boundary region, from which the domain boundary structure can be distinctly distinguished. Fig. 2i is enlarged view of the framed area I (domain interior) in Fig. 2d and shows that it has a similarly ideal atom configuration of GeTe. More elaborate structure can be observed in the ABF-STEM image in Fig. 2e, and the domain boundary consists of the middle layer probably occupied by Cu atoms (details in Fig. 2k) and two vacancy layers on both sides, which can be considered as a sandwich-like structure. To our knowledge, it is the first time to identify such a unique domain boundary structure in GeTe-based materials, which is different with the observed results in previous studies [32,36,37,39]. Fig. 2h is the intensity profile along the arrow in Fig. 2d, in which the high- and low-intensity peaks are due to heavier (Te) and lighter (Ge or Cu) atomic columns, respectively. Correspondingly, the observed planar vacancy layers are on account of the missing of Ge atomic planes [37,43], confirming the sandwich-like stacking faults structure of the domain boundary.

To verify whether this unique sandwich-like structure is universal in crystal, Fig. 2j is a selected HAADF-STEM image to show that several groups of it aggregate in local area nearby the domain boundary. The corresponding FFT electron diffraction pattern is shown in Fig. 2g, and the spots in the circle brighten markedly resulting from the aggregated sandwich-like structures, which is distinctly different from Fig. 2f derived from the area containing only one of such structure. Further, the specific defect structure in marked region II is magnified as Fig. 2k. It can be easily observed from the contrast that two atoms occupy a Ge vacancy in the interspace between two contiguous Te atomic planes, along with one vacancy layer on each side. Considering Sb atoms only replace Ge atoms, and recent calculation studies reveal that, the formation energy of two Cu atoms replacing one Ge atom by forming a substitutional-interstitial defect pair is lowest [38], so it is reasonably assumed that two layers of Cu atoms occupy the Ge vacancy layer in this work, thus forming a "vacancy/Cu–Cu/vacancy" sandwich-like structure. On the other hand, the anionic Te layer is slightly changed by the sandwich-like structure, the planar spacing across vacancy layer is about 3.3 Å and the spacing across Cu occupied layer is about 4.4 Å, while the Te layer spacing in GeTe matrix is about 3.8 Å. Although the lattice shows a slight transformation trend toward hexagonal Cu_2Te structure, in which two kinds of Te layer spacing are 2.8 Å and 4.5 Å respectively [45], the Te framework is well maintained along with the GeTe matrix, which could simultaneously facilitate carrier transport while increase phonon scatterings.

The modulation of Ge vacancy layers to sandwich-like stacking faults intrinsically influences the transportation of carriers and phonons. Electrical conductivity, Seebeck coefficient and carrier concentration of series of $Ge_{1-x-y}Cu_{2x}Sb_yTe$ samples were measured, as shown in Fig. 3a–c. A significant decrease of carrier concentration from ~10^{21} cm^{-3} to 3×10^{20} cm^{-3} is achieved with x ~3%, proving that Cu_2Te is a more effective dopant in GeTe comparing with Sb/Bi doping [32,33,41]. The reason why carrier concentration decreases dramatically in $Ge_{1-x}Cu_{2x}Te$ is mainly attributed to vanishment of Ge vacancy layers as observed in TEM images. Thus, the Seebeck coefficient for $Ge_{0.97}Cu_{0.06}Te$ is enhanced to 60 μV K^{-1} from 30.4 μV K^{-1} in GeTe.

Importantly, since excess Cu doping is more effective to suppress the formation of Ge vacancy defects, the total concentration of defects, including point defects and stacking faults defects, is greatly reduced, which significantly weaken the scattering effect on carriers. Similar to the case in GeTe-$x$$Cu_2Te$-$y$BiTe solid solution [38], the carrier mobility is upgraded to ~100 cm^2 V^{-1} s^{-1} in $Ge_{0.97}Cu_{0.06}Te$ sample, which is more superb than that of most reported GeTe materials [10,37,40,43]. Therefore, a relatively high PF of ~22 μW m^{-1} K^{-2} is obtained at 300 K as shown in Fig. S5 in contrast to that of pristine GeTe or others with similar carrier concentration [11,30,40,41]. Further Sb doping can reduce carrier concentration to a sufficiently low level, $\sim 1 \times 10^{20}$ cm^{-3}. Since Sb doping introduces more points defects and also may decrease the formation energy of Ge vacancy [32,37], the mobility in (Cu,Sb) co-doping samples slightly declines comparing with $Ge_{1-2x}Cu_{2x}Te$ samples. Nevertheless, the mobility of $Ge_{0.97-y}Cu_{0.06}Sb_yTe$ compound with $y = 0.08$ still retains a value of 49.6 cm^2 V^{-1} s^{-1}, which is much higher than the Sb-doped or Bi-doped GeTe materials (Fig. 3e). In addition, the mobility in this work is only lower than that of GeTe-$x$$Cu_2Te$-$y$BiTe alloys [38], which may result from the relatively low effective mass ~1.0 m_0.

Fig. 3d displays room temperature Hall carrier concentration dependent Seebeck coefficient for current $Ge_{1-x-y}Cu_{2x}Sb_yTe$ compounds. The solid red and blue curves describe single parabolic band model prediction of Seebeck coefficient versus carrier concentration, based on acoustic phonon dominant scattering mechanism which is demonstrated by the $T^{-3/2}$ dependence of carrier mobility near 300 K as shown in Fig. S7. As can be seen from the Pisarenko plot, the experimental Seebeck coefficient of $Ge_{1-x}Cu_{2x}Te$ samples basically falls well on the red

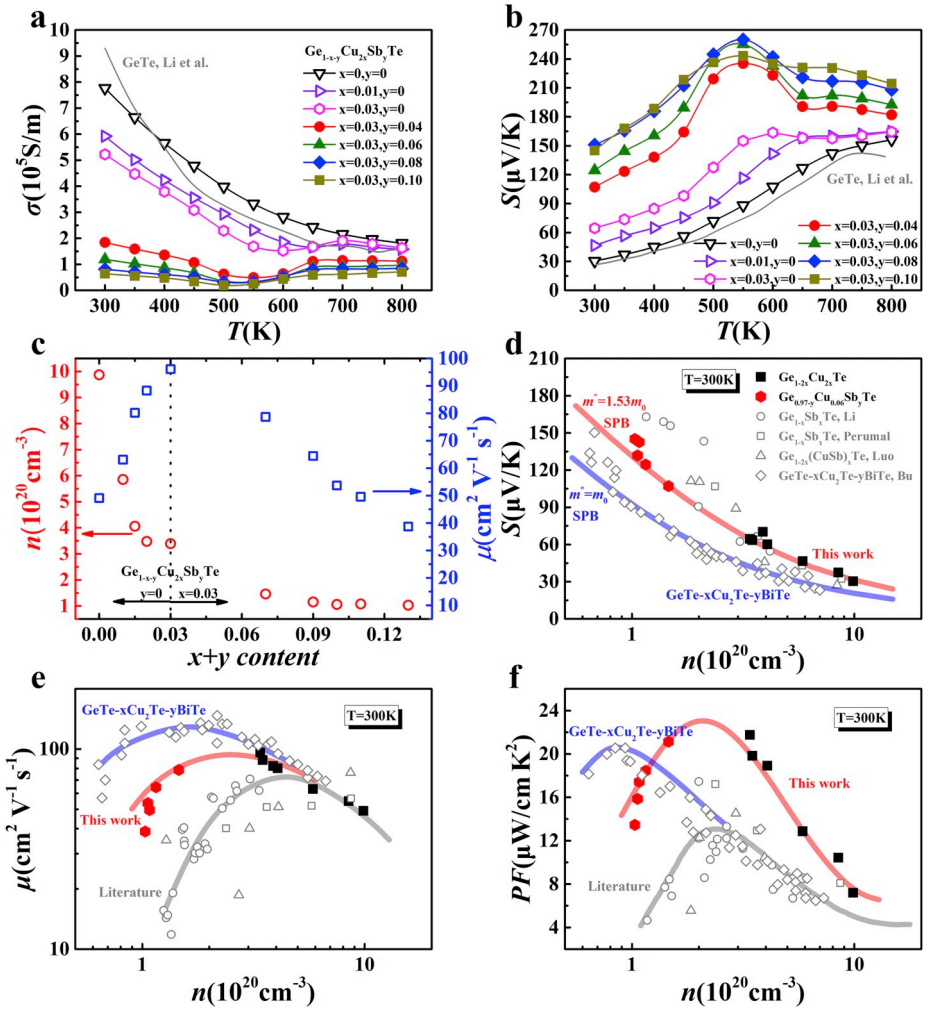

Fig. 3. Temperature dependence of (a) electrical conductivity, (b) Seebeck coefficient and (c) Composition dependence of Hall carrier concentration and Hall mobility, as well as Hall carrier concentration dependent (d) Seebeck coefficient, (e) carrier mobility, and (f) power factor for $Ge_{1-x-y}Cu_{2x}Sb_yTe$ compounds at room temperature, with a comparison to literature results of GeTe based materials [11,32,38,41]. Curves are used to guide the eyes unless specially noted.

prediction curve with density of state effective mass $m_d^* = 1.53\ m_0$, indicating that alloying has a negligible influence on band structure, consistent with other Cu doped GeTe literatures [11,30,38]. With further Sb doping, the m_d^* gradually increases to 1.80 m_0. This is presumably because Sb doping can promote crystal symmetry to be more cubic [32,41], as shown in XRD patterns and interaxial angles, leading to a slightly enhanced band convergence. The basically well-maintained band structure of GeTe and impressively high mobility guarantee the splendid electrical transport properties, and the room temperature power factor in this work is higher than most of literatures as shown in Fig. 3f [11,32,41].

Meanwhile, the depression of Ge vacancy layer does not lead to weakness of phonon scattering. Fig. 4a and b show temperature dependence of total thermal conductivity and lattice thermal conductivity for $Ge_{1-x-y}Cu_{2x}Sb_yTe$ compounds. The lattice thermal conductivity κ_L are calculated by subtracting electronic thermal conductivity κ_e from total thermal conductivity κ, which can be calculated based on Wiedeman-Franz law (i.e., $\kappa_e = L\sigma T$, where L is Lorenz number shown in Fig. S6, estimated by the single parabolic band model). With Sb and excess Cu doping, the total thermal conductivity are basically reduced comparing with pristine GeTe. With the increase of Sb doping amount from $y = 0.04$ to $y = 0.10$, the lowest value of lattice thermal conductivity ~1.25 W m^{-1} K^{-1} is achieved for $Ge_{0.89}Cu_{0.06}Sb_{0.08}Te$ at room temperature. At 800 K, the lattice thermal conductivities of all samples doped with Cu and Sb are at a very low level, ~0.38–0.58 W m^{-1} K^{-1}, which are almost the minimum value reported in Sb or Bi doped GeTe literatures [32,33,39,41]. And these are comparable or even lower than the minimum lattice thermal conductivity of 0.45 W m^{-1} K^{-1} for GeTe, calculated on the basis of Cahill model [46].

To explore the effect of stacking-faults modulation on reducing lattice thermal conductivity κ_L, the lattice thermal conductivity in the low temperature range (5–300 K) are investigated using Debye-Callaway model by taking into account several different phonon scattering mechanisms including Umklapp processes (U), grain boundaries (B), point defects (PD) and stacking faults (SF), as shown in Fig. 4c. The fitting curves are in good agreement with the experimental data with R^2 exceeding 99%. Specifically, the phonon scattering parameter of stacking faults can be expressed as following equation:

$$C = 0.7\frac{a^2\gamma^2 N_s}{\nu_s} \quad (1)$$

where a is the average lattice parameter, γ is the Gruneisen parameter, ν_s is average sound speed, N_s is the number of stacking faults in a line of unit length. The scattering parameter of stacking faults in $Ge_{0.99}Cu_{0.02}Te$ is enhanced comparing with pure GeTe as shown in Table S1, and scattering parameter in current $Ge_{0.93}Cu_{0.06}Sb_{0.04}Te$ is also higher than reported Bi-doped sample with similar doping content [37]. According to Equation (1), the value of scattering parameter varies linearly with the concentration of stacking faults N_s, however, the concentration of Ge

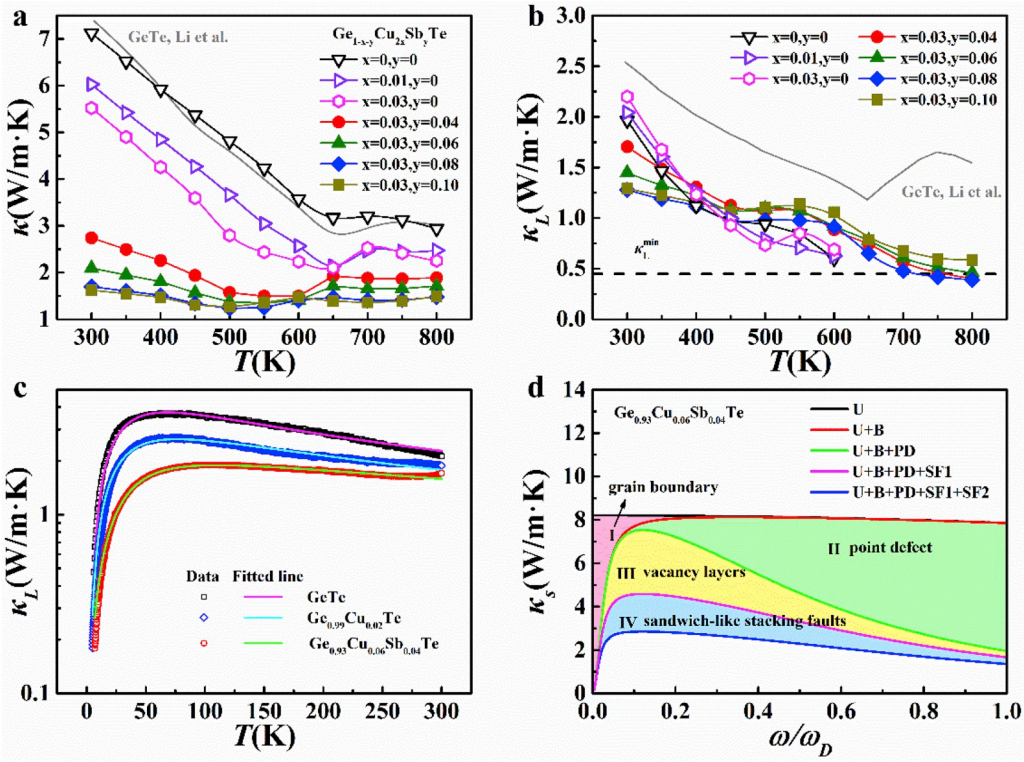

Fig. 4. Temperature dependence of (a) total thermal conductivity, (b) lattice thermal conductivity for $Ge_{1-x-y}Cu_{2x}Sb_yTe$. (c) Experimental data and fitting of lattice thermal conductivity in the low temperature range (5–300 K) by Debye-Callaway model. (d) Calculated spectral lattice thermal conductivity (κ_s) using Debye-Callway model with various phonon scattering mechanisms including Umklapp processes (U), grain boundaries (B), point defects (PD), and stacking faults (SF) at 300 K.

vacancy layers is reduced in $Ge_{1-x-y}Cu_{2x}Sb_yTe$ based on TEM investigation result. So the scattering effect of sandwich-like structure needs to be taken into particular consideration. In fact, the phonon scattering effect caused by stacking faults depends on the perpendicular dimension of 2D defects and their concentration [47], the sandwich-like structure with the total dimension of 11 Å is expected to scatter the phonons more strongly than the simple one-fold Ge vacancy layer. Thus, the scattering parameters of Ge vacancy layers and sandwich-like stacking faults are separated, and the concentration of two kinds of stacking faults are calculated in Table S2, respectively. Comparing to the previously reported Bi-doped samples [37,43], with excess Cu doping, the concentration of Ge vacancy layers is indeed depressed, consistent with TEM results. But the involved sandwich-like stacking faults with lower concentration provide increased contribution of phonon scattering, proving that the sandwich-like stacking faults are more effective on scattering phonons comparing with the simple Ge vacancy layers.

Considering various phonon scattering processes, the spectral lattice thermal conductivity κ_s versus phonon frequency ω is calculated as shown in Fig. 4d. Since the integral of κ_s with regard to phonon frequency is equal to corresponding κ_L, the area between two adjacent curves represents the reduction of κ_L caused by introducing another phonon scattering center. As can be easily seen from Fig. 4d, since the two kinds of stacking faults have the same frequency dependent relation, they contribute a large scattering effect on phonons in the similar broad range of frequency (Area III and Area IV), which leads to extremely low lattice thermal conductivity in current study.

As mentioned above, the presence of special sandwich-like stacking faults provides the possibility of simultaneously realizing good electrical performance and ultralow lattice thermal conductivity, which would undoubtedly lead to good thermoelectric properties. As a result, the zT values of (Cu, Sb) co-doped GeTe samples are greatly enhanced, and the highest zT value for $Ge_{0.89}Cu_{0.06}Sb_{0.08}Te$ is 2.04 at 750 K. Besides, the maximum zT_{ave} value of 1.35 is also achieved in the same sample over the medium temperature range (400–800 K), which is better than several state-of-the-art GeTe-based materials reported before. And the thermoelectric performance of the sample with highest zT value is highly reproducible, according to the repeated measurements (Figs. S10 and S11).

4. Summary

In this work, we systematically investigated the microstructure and TE properties of $Ge_{1-x-y}Cu_{2x}Sb_yTe$ materials. Cs-corrected TEM investigation reveals that, two layers of Cu atoms occupy the single Ge vacancy layer in the excess Cu doped GeTe material, forming a "vacancy/Cu–Cu/vacancy" sandwich-like structure. Meanwhile, the concentration of the intrinsic Ge vacancy layers significantly decreases, which can greatly weaken the scattering of carriers. Thus, a high carrier mobility ~100 $cm^2 V^{-1} s^{-1}$ is obtained, leading to significantly improved power factor at room temperature. Further, by fitting the low temperature lattice thermal conductivity, the scattering parameters of sandwich-like stacking faults and Ge vacancy layers are respectively evaluated. And the result demonstrates that the sandwich-like stacking faults with large dimension can scatter wide frequency phonons more strongly than simple one-fold Ge vacancy layer. Therefore, an extremely low lattice thermal conductivity of 0.38 W $m^{-1} K^{-1}$ has been achieved, approaching the theoretical amorphous limit of GeTe. Consequently, a highest zT value > 2.0 and zT_{ave} value of 1.35 are obtained in this work. Considering carrier mobility is not a function of band degeneracy to some extent, further improvements of thermoelectric performance can be expected if band convergence is achieved. This work realizes the modulation of 2D stacking faults for adjusting the scattering effect of electrons and phonons, and makes up the important piece of multi-scale microstructure tailoring for TE materials.

Declaration of competing interest

The authors declare that they have no known competing financial interests or personal relationships that could have appeared to influence the work reported in this paper.

Acknowledgements

The work was financially supported by the National Key Research and Development Program of China (Grant No. 2018YFB0703604), the National Natural Science Foundation of China (NSFC) (Grant Nos.51632010, 51572282 and 51972324), and Youth Innovation Promotion Association CAS (No. 2019253).

Appendix A. Supplementary data

Supplementary data to this article can be found online at https://doi.org/10.1016/j.nanoen.2019.104347.

References

[1] L.E. Bell, Science 321 (2008) 1457–1461.
[2] X. Shi, L. Chen, Nat. Mater. 15 (2016) 691–692.
[3] I. Petsagkourakis, K. Tybrandt, X. Crispin, I. Ohkubo, N. Satoh, T. Mori, Sci. Technol. Adv. Mater. 19 (2018) 836–862.
[4] C. Dagdeviren, Z. Li, Z.L. Wang, Annu. Rev. Biomed. Eng. 19 (2017) 85–108.
[5] A.F. Ioffe, Semiconductor Thermoelements and Thermoelectric Cooling, Infosearch, London, 1957.
[6] W. Zhao, Z. Liu, Z. Sun, Q. Zhang, P. Wei, X. Mu, H. Zhou, C. Li, S. Ma, D. He, P. Ji, W. Zhu, X. Nie, X. Su, X. Tang, B. Shen, X. Dong, J. Yang, Y. Liu, J. Shi, Nature 549 (2017) 247–251.
[7] Y. Xiao, H. Wu, W. Li, M. Yin, Y. Pei, Y. Zhang, L. Fu, Y. Chen, S.J. Pennycook, L. Huang, J. He, L.D. Zhao, J. Am. Chem. Soc. 139 (2017) 18732–18738.
[8] H. Wu, C. Chang, D. Feng, Y. Xiao, X. Zhang, Y. Pei, L. Zheng, D. Wu, S. Gong, Y. Chen, J. He, M.G. Kanatzidis, L.-D. Zhao, Energy Environ. Sci. 8 (2015) 3298–3312.
[9] T. Zhu, Y. Liu, C. Fu, J.P. Heremans, J.G. Snyder, X. Zhao, Adv. Mater. 29 (2017) 1605884.
[10] J. Li, Z. Chen, X. Zhang, H. Yu, Z. Wu, H. Xie, Y. Chen, Y. Pei, Adv. Sci. (Weinh) 4 (2017) 1700341.
[11] L. Yue, T. Fang, S. Zheng, W. Cui, Y. Wu, S. Chang, L. Wang, P. Bai, H. Zhao, ACS Appl. Energy Mater. 2 (2019) 2596–2603.
[12] Y. Pei, X. Shi, A. LaLonde, H. Wang, L. Chen, G.J. Snyder, Nature 473 (2011) 66–69.
[13] J.P. Heremans, V. Jovovic, E.S. Toberer, A. Saramat, K. Kurosaki, A. Charoenphakdee, S. Yamanaka, G.J. Snyder, Science 321 (2008) 554–557.
[14] K. Biswas, J. He, I.D. Blum, C.I. Wu, T.P. Hogan, D.N. Seidman, V.P. Dravid, M. G. Kanatzidis, Nature 489 (2012) 414–418.
[15] M. Samanta, K. Biswas, J. Am. Chem. Soc. 139 (2017) 9382–9391.
[16] Z. Zheng, X. Su, R. Deng, C. Stoumpos, H. Xie, W. Liu, Y. Yan, S. Hao, C. Uher, C. Wolverton, M.G. Kanatzidis, X. Tang, J. Am. Chem. Soc. 140 (2018) 2673–2686.
[17] X. Zhang, J. Li, X. Wang, Z. Chen, J. Mao, Y. Chen, Y. Pei, J. Am. Chem. Soc. 140 (2018) 15883–15888.
[18] W. Li, L. Zheng, B. Ge, S. Lin, X. Zhang, Z. Chen, Y. Chang, Y. Pei, Adv. Mater. 29 (2017) 1605887.
[19] J. Dong, F.-H. Sun, H. Tang, J. Pei, H.-L. Zhuang, H.-H. Hu, B.-P. Zhang, Y. Pan, J.-F. Li, Energy Environ. Sci. 12 (2019) 1396–1403.
[20] S.I. Kim, K.H. Lee, H.A. Mun, H.S. Kim, S.W. Hwang, J.W. Roh, D.J. Yang, W. H. Shin, X.S. Li, Y.H. Lee, G.J. Snyder, S.W. Kim, Science 348 (2015) 109–114.
[21] Z. Chen, B. Ge, W. Li, S. Lin, J. Shen, Y. Chang, R. Hanus, G.J. Snyder, Y. Pei, Nat. Commun. 8 (2017) 13828.
[22] R. Venkatasubramanian, E. Siivola, T. Colpitts, B. O'quinn, Nature 413 (2001) 597–602.
[23] J. Mao, Y. Wang, H.S. Kim, Z. Liu, U. Saparamadu, F. Tian, K. Dahal, J. Sun, S. Chen, W. Liu, Z. Ren, Nano Energy 17 (2015) 279–289.
[24] Y. Yu, D.-S. He, S. Zhang, O. Cojocaru-Mirédin, T. Schwarz, A. Stoffers, X.-Y. Wang, S. Zheng, B. Zhu, C. Scheu, D. Wu, J.-Q. He, M. Wuttig, Z.-Y. Huang, F.-Q. Zu, Nano Energy 37 (2017) 203–213.
[25] K. Biswas, J. He, Q. Zhang, G. Wang, C. Uher, V.P. Dravid, M.G. Kanatzidis, Nat. Chem. 3 (2011) 160–166.
[26] C.J. Vineis, A. Shakouri, A. Majumdar, M.G. Kanatzidis, Adv. Mater. 22 (2010) 3970–3980.
[27] A.U. Khan, K. Kobayashi, D.-M. Tang, Y. Yamauchi, K. Hasegawa, M. Mitome, Y. Xue, B. Jiang, K. Tsuchiya, D. Golberg, Y. Bando, T. Mori, Nano Energy 31 (2017) 152–159.
[28] J. Li, X. Zhang, X. Wang, Z. Bu, L. Zheng, B. Zhou, F. Xiong, Y. Chen, Y. Pei, J. Am. Chem. Soc. 140 (2018) 16190–16197.
[29] S. Perumal, S. Roychowdhury, K. Biswas, J. Mater. Chem. C 4 (2016) 7520–7536.
[30] S. Shimano, Y. Tokura, Y. Taguchi, Apl. Mater. 5 (2017), 056103.
[31] M. Hong, Y. Wang, T. Feng, Q. Sun, S. Xu, S. Matsumura, S.T. Pantelides, J. Zou, Z. G. Chen, J. Am. Chem. Soc. 141 (2019) 1742–1748.
[32] S. Perunnal, S. Roychowdhury, D.S. Negi, R. Datta, K. Biswas, Chem. Mater. 27 (2015) 7171–7178.
[33] S. Perumal, S. Roychowdhury, K. Biswas, Inorg. Chem. Front. 3 (2016) 125–132.
[34] S. Perumal, P. Bellare, U.S. Shenoy, U.V. Waghmare, K. Biswas, Chem. Mater. 29 (2017) 10426–10435.
[35] T. Xing, Q. Song, P. Qiu, Q. Zhang, X. Xia, J. Liao, R. Liu, H. Huang, J. Yang, S. Bai, D. Ren, X. Shi, L. Chen, Natl. Sci. Rev., DOI:10.1093/nsr/nwz052.
[36] M. Hong, Z.G. Chen, L. Yang, Y.C. Zou, M.S. Dargusch, H. Wang, J. Zou, Adv. Mater. 30 (2018) 1705942.
[37] M. Hong, Y. Wang, W. Liu, S. Matsumura, H. Wang, J. Zou, Z.-G. Chen, Adv. Energy Mater. 8 (2018) 1801837.
[38] Z. Bu, W. Li, J. Li, X. Zhang, J. Mao, Y. Chen, Y. Pei, Mater. Today Phys. (2019) 100096.
[39] Z.H. Liu, J.F. Sun, J. Mao, H.T. Zhu, W.Y. Ren, J.C. Zhou, Z.M. Wang, D.J. Singh, J. H. Sui, C.W. Chu, Z.F. Ren, Proc. Natl. Acad. Sci. U.S.A. 115 (2018) 5332–5337.
[40] D. Wu, L.D. Zhao, S. Hao, Q. Jiang, F. Zheng, J.W. Doak, H. Wu, H. Chi, Y. Gelbstein, C. Uher, C. Wolverton, M. Kanatzidis, J. He, J. Am. Chem. Soc. 136 (2014) 11412–11419.
[41] J. Li, X. Zhang, S. Lin, Z. Chen, Y. Pei, Chem. Mater. 29 (2016) 605–611.
[42] H.S. Lee, B.-S. Kim, C.-W. Cho, M.-W. Oh, B.-K. Min, S.-D. Park, H.-W. Lee, Acta Mater. 91 (2015) 83–90.
[43] J. Li, Y. Xie, C. Zhang, K. Ma, F. Liu, W. Ao, Y. Li, C. Zhang, ACS Appl. Mater. Interfaces 11 (2019) 20064–20072.
[44] K.S. Bayikadi, R. Sankar, C.T. Wu, C. Xia, Y. Chen, L.-C. Chen, K.-H. Chen, F.-C. Chou, J. Mater. Chem. A 7 (2019) 15181–15189.
[45] Y. He, T. Zhang, X. Shi, S.-H. Wei, L. Chen, NPG Asia Mater. 7 (2015) e210-e210.
[46] D.G. Cahill, S.K. Watson, R.O. Pohl, Phys. Rev. B 46 (1992) 6131–6140.
[47] P.G. Klemens, Can. J. Phys. 35 (1957) 441–450.

Li Xie is currently a Ph.D. candidate in the Shanghai Institute of Ceramics, Chinese Academy of Sciences, China. He received his Bachelor degree from Wuhan University of Technology, China. His current research mainly focuses on high performance GeTe based thermoelectric materials and devices.

Yongjin Chen is currently a postdoctoral research fellow in the Center for High Pressure Science &Technology Advanced Research. He received a B.E. from Sichuan University, and a Ph. D. degree from the Beijing University of Technology in 2019. His research focuses on advanced transmission electron microscopy techniques, energy related materials and phase change memory materials.

Dr. Ruiheng Liu received his bachelor degree from Shandong University in 2007, and his Ph.D. degree in Materials Physics & Chemistry from Chinese Academy of Sciences in 2012. His research activities primarily focus on the novel transport mechanism of thermoelectric semiconductors, thermodynamics of materials and interfaces, design and fabrication of high performance TE devices.

Erhong Song received his Ph.D. degree in department of Materials Science and Engineering, Jilin University, Changchun, P. R. China. He is currently an Assistant Professor of Shanghai Institute of Ceramics, Chinese Academy of Sciences. His research interests include heterogenous catalytic reactions, Li-battery and nano advanced energy materials.

Tong Xing is currently a Ph.D. candidate in the Shanghai Institute of Ceramics, Chinese Academy of Sciences, China. She received her Bachelor degree from Yanshan University, China. Her current research mainly focuses on high performance GeTe based thermoelectric materials and devices.

Tingting Deng is currently a Ph.D. candidate supervised by Prof. Lidong Chen at Shanghai Institute of Ceramics Chinese Academy of Sciences, and the major is Material Physics and Chemistry. She received her Bachelor's degree from Zhengzhou University in 2015, and the major was Inorganic Non-Metallic Materials. Her research direction is mainly focused on thermoelectric materials (TE) in ternary Cu–Sn–S system.

Dr. Qingfeng Song is currently a research assistant in the State Key Laboratory of High Performance Ceramics and Superfine Microstructure, Shanghai Institute of Ceramics, Chinese Academy of Sciences. He received his B.S. degree from the Hefei University of Technology in 2013 and Ph.D. from the University of Chinese Academy of Sciences in 2019. His current research interest focuses on low-temperature thermoelectric materials and devices.

Jianjun Liu is a professor in Computational Materials Sciences at the Shanghai Institute of Ceramics, Chinese Academy of Science (CAS). His research interests include computational simulation on energy conversion and storage materials with an aim to reveal the relation of structure and properties, further design/optimize novel and high-performance materials.

Prof. Renkui Zheng received his Ph.D. degree from the University of Science and Technology of China (USTC) in 2003. Then he joined Department of Applied Physics, The Hong Kong Polytechnic University as a post-doctoral fellow. From 2009, he worked as an Alexander von Humboldt fellow at the Max-Planck Institute for Solid State Research at Stuttgart, Germany. In 2011, he joined the Shanghai Institute of Ceramics, Chinese Academy of Sciences. His current research focuses on the electronic and magnetic properties of quantum materials and complex oxide thin films as well as magnetoelectric coupling effects of multiferroic composites.

Xiang Gao received his Ph.D. in 2011 from the Shanghai Institute of Ceramics, Chinese Academy of Sciences. He became a principal investigator at the Center for High Pressure Science and Technology Advanced Research (HPSTAR) in 2018. His research interests focus on the microstructure sciences and engineering of advanced functional materials.

Dr. Shengqiang Bai, received his bachelor degree from Zhejiang University in 2001, and his Ph.D. degree in Materials Physics & Chemistry from Chinese Academy of Sciences in 2010. In 2001 he joined Shanghai Institute of Ceramics and was promoted to professor in 2017. His research activities primarily involve the mass production of high performance thermoelectric materials including skutterudites, half-Heusler, SiGe-based alloys and other new TE materials; design and fabrication of TE devices; evaluation and service behavior of TE devices; and also the applications of TE devices. He received the 2nd Prize of National Award for Technological Invention in 2014.

Professor Lidong Chen received his Ph.D. from Tohoku University in Japan (1990). Since 1990, he had worked in Riken Corporation (Chief Engineer), National Aerospace Laboratory, Tohoku University (Associate Professor) and University of Michigan (Visiting Scholar). He joined Shanghai Institute of Ceramics, Chinese Academy of Sciences (SICCAS) as a professor in 2001. At present, he is the director of State Key Lab of High Performance Ceramics and Superfine Microstructures. His research focuses on advanced thermoelectric (TE) materials and devices.